International Journal of Physical Sciences

Volume 10 Number 19 16 October 2015

ISSN 1992-1950

Academic Journals

ABOUT IJPS

The **International Journal of Physical Sciences (IJPS)** is published weekly (one volume per year) by Academic Journals.

International Journal of Physical Sciences (IJPS) is an open access journal that publishes high-quality solicited and unsolicited articles, in English, in all Physics and chemistry including artificial intelligence, neural processing, nuclear and particle physics, geophysics, physics in medicine and biology, plasma physics, semiconductor science and technology, wireless and optical communications, materials science, energy and fuels, environmental science and technology, combinatorial chemistry, natural products, molecular therapeutics, geochemistry, cement and concrete research, metallurgy, crystallography and computer-aided materials design. All articles published in IJPS are peer-reviewed.

Contact Us

Editorial Office: ijps@academicjournals.org

Help Desk: helpdesk@academicjournals.org

Website: http://www.academicjournals.org/journal/IJPS

Submit manuscript online http://ms.academicjournals.me/

Editorial Board

International Journal of Physical Sciences

Table of Contents: Volume 10 Number 19, 16 October, 2015

ARTICLES

academicJournals

Vol. 10(19), pp. 537-542, 16 October, 2015
DOI: 10.5897/IJPS2015.4399
Article Number: 76D3F7B55705
ISSN 1992 - 1950

http://www.academicjournals.org/IJPS

International Journal of Physical Sciences

Full Length Research Paper

Crystal size effect on the photoluminescence of calcium aluminate doped Mn^{2+} nanocrystals

Jubu P. Rex[1]*, Abutu A. Nathan[1] and Mbah Vitalis[2]

[1]Department of Physics, University of Agriculture, Makurdi, Benue State, Nigeria.
[2]Department of Science Laboratory Technology, Federal Polytechnic, Nasarawa, Nasarawa State, Nigeria.

Received 15 August, 2015; Accepted 2 October, 2015

Research into finding environmentally friendly, efficient and economic viable nanophosphors is still ongoing as the incorporation of radioactive substances into phosphors to improve their short time luminescence poses serious environmental concern. The present paper investigates the effect of particle size on the, morphology and photoluminescence of environmentally friendly $CaAl_2O_4$: Mn^{2+} nanocrystals. The phosphor was prepared by the high temperature reaction technique. X-ray diffraction analysis revealed monoclinic structure. Average crystal size of the unpassivated nanomaterial (CAU) was found to be higher (41.49 nm) than that of the passivated (CAP) one (34.81 nm). Photoluminescence investigation at 345 nm excitation showed emission wavelengths that match Mn^{2+} emission. Both the emission color and intensity of the nanocrystals were observed to be crystal-size dependent with high luminescence intensity and deep blue emission peaks coming from CAP; while low luminescence intensity, prominent violet peaks and a weak blue emission peak were registered on CAU. Investigation of the samples responds to different excitation wavelengths revealed that both materials received corresponding colour emission and maximum intensity at 465 nm excitation.

Key words: Photoluminescence, morphology, passivation, fluorescence phosphor.

INTRODUCTION

Last two decades have witnessed a rapid advancement in various techniques for the fabrication of nanoparticles (Senapati et al., 2013). The interest in semiconductor nanoparticles is justified by the fact that their fundamental physical and chemical properties can be very different from those of bulk materials. The advantages of nanoparticles over their bulk counterparts include small particle size with large surface area, improved optical, electrical and mechanical properties. According to Kelvil (2013), nanoparticles have the advantage over bulk materials due to their surface plasmon response, enhanced Rayleigh scattering and surface enhanced Raman scattering in metal nanoparticle and their quantum size effect in semiconductors and supermagnetism in magnetic materials. The II-VI nanostructures with their distinct optical and electrical properties due to their two-dimensional confinement and anisotropic shape have become potential candidates for application in electronics, optoelectronics, lasers and environmental control (Sugaderan, 2013; Kenanakis et al., 2007; Mou et

*Corresponding author. E-mail: jubu_raphael@yahoo.com

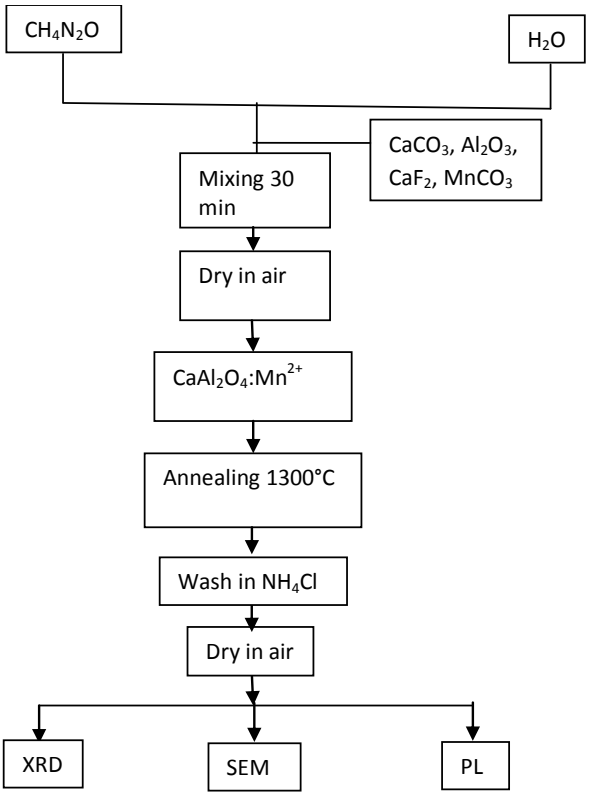

Figure 1. Summary of synthesis and characterization of nanoparticles.

al., 2012).

Nanostructures have been successfully synthesized by various methods like chemical or physical vapour deposition, thermal evaporation, magnetron sputtering, laser ablation, hydrothermal method, spray pyrolysis, catalyst-mediated organization, electrodeposition, homogeneous precipitation, solvothermal synthesis, sonochemical process and sol-gel process (Amita and Srivastava, 2011). Amongst these methods, monocalcium aluminate ($CaAl_2O_4$) have been successfully prepared by solution combustion method (Vijay et al., 2007; Nguyen et al., 2004; Ali, 2011; Dejene et al., 2010), hydrazine assisted self-combustion (Satapathy and Mishra, 2014), sol-gel and solid state method (Toumas et al., 2012; Jagjeet et al., 2002; Madhukumar et al., 2006; Bo et al., 2005; Rivas et al., 2004). But the use of urea in solid state synthesis has been negligible.

The role of urea (CH_4N_2O) in the development of blue-emitting monocalcium aluminate nanoparticles was to tailor the structural, morphological and luminescence properties of the nanomaterial. Urea finds several roles in the preparation of nanomaterials. For example, urea is used as a flux by many researchers to promote the formation of a good crystalline phase system (Haranath et al., 2010). Urea is used as a popular fuel for producing highly uniform, complex oxide ceramic powders with precisely controlled stoichiometry (Christine et al., 2010). Exothermic redox reaction occurs between fuel and oxidizers (nitrates) (Toniolo et al., 2005) which generate high temperature in the reaction.

In the present paper, we investigated the morphology, crystal structure and size, and photoluminescence emission behavior of $CaAl_2O_4:Mn^{2+}$ nanocrystals prepared by slurry. Solid state diffusion is the most popular method for the preparation of nanophosphors even at commercial scale (Kartik et al., 2012). The monocalcium aluminate was doped to introduce new properties by changing the mass transport properties (Saeid et al., 2012). Fluorescence phosphors like $CaAl_2O_4$, $BaMgAl_{12}O_{19}$, SrAl2B2O7 finds application in light emitting devices, plasma display panels, medical lamps and fluorescent lamps (Haranath et al., 2010). Our success in this research is anchored on the reduction of crystallite size of the nanoparticles synthesized by the high temperature reaction using urea as passivating agent; knowing that reduced particle size and hence large surface area, enhances photoluminescence mechanism by providing reinforcement and catalytic effect. (Ali, 2011) asserts that when the diameter of a particle is reduced the band gap is blue-shifted due to the effect of quantum confinement.

MATERIALS AND METHODS

The requisite materials used for the successful execution of the research include the following. Calcium carbonate ($CaCO_3$), aluminum oxide (Al_2O_3), manganese carbonate ($MnCO_3$), calcium fluoride (CaF_2), ammonium chloride (NH_4Cl), pure urea (CH_4N_2O), distilled water and muffle furnace. All chemicals are of analytical grade and where used without further purification. Chemicals were purchased from Suzhou Yacoo Chemical Reagent Co. Ltd, China.

In this present study, the nanomaterial was prepared according to the chemical formula $Ca_{0.2}Al_2O_4:Mn_{0.004}$. All the precursors were of analytical grade and were used without further purification. In order to study the effect of urea on the nanoparticles, two samples were prepared. Sample CAU was prepared by slurring $CaCO_3$, Al_2O_3, CaF_2, and $MnCO_3$ in distilled water for 20 min and left to dry in air. The resulting powder was grounded into fine particles using pestle and mortar. Muffle furnace was used to maintain the crucibles containing the samples at 1300°C for 1 h in order to cause changes in the physical and chemical constitution of the nanomaterials and also to drive off carbon dioxide. Sample CAP was synthesized in a similar way though by slurring the precursors in a solution of 2.0g urea in order to reduce the crystal size of the nanomaterial. Both samples, CAU and CAP were washed in 0.25l of water using 4.0g ammonium chloride to extract the impurities and left to dry in air.

Characterization of the nanocrystals was carried out using X-ray diffractometer PW3050/60 at the Sheda of Science and Technology Abuja, Nigeria. The nature and form of the material was studied using scanning electron microscope an oxford instrument at the Amadu Bello University Zaria, Nigeria. The photoluminescence property was examined using photoluminescence spectrometer model Perkin-Elmer LS-55 domiciled at National Centre for Nanostructured Materials (CSIR), Pretoria, South Africa.

The chemical reactions leading to the synthesis process are as presented in equations 1 to 3 while the flowchart showing summary of the synthesis is presented in Figure 1.

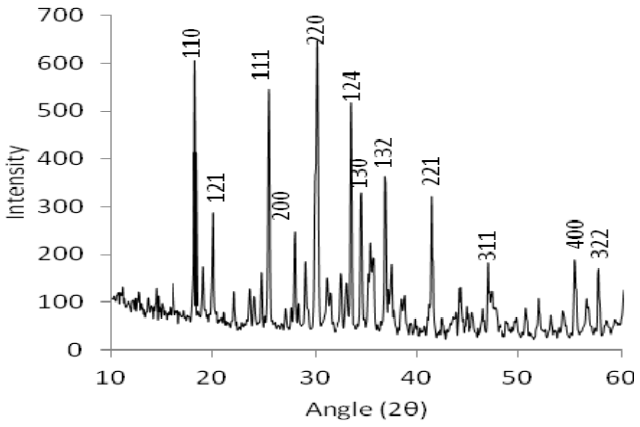

Figure 2a. XRD pattern of CAP

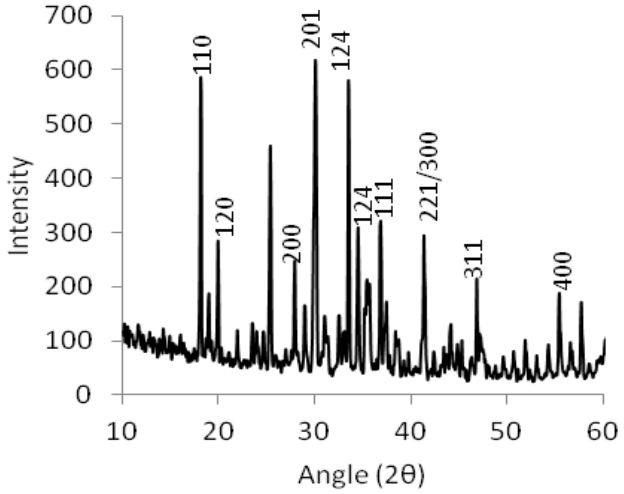

Figure 2b. XRD pattern of CAU.

$$CaCO_3 + Al_2O_3 \rightarrow CaAl_2O_4 + CO_2 \quad (1)$$

$$CaAl_2O_4 + CaF_2 \rightarrow Ca_2Al_2O_4 + F_2 \quad (2)$$

$$Ca_2Al_2O_4 + MnCO_3 \rightarrow CaAl_2O_4{:}Mn + CO_2 + CaO \quad (3)$$

Crystal size of the nanoparticles was calculated using Debye Scherrer formula which states that

$$D = \frac{0.9\lambda}{\beta \cos\theta} \quad (4)$$

where D is the crystallite size, λ is wavelength of the X-ray source in nm, β is the full width at half maximum (FWHM) in radians, and θ is the angle of diffraction in radians.

The strain of the nanoparticles was calculated from Stokes-Wilson equation:

$$\epsilon_{str} = \frac{\beta \cot\theta}{4} \quad (5)$$

where β is FWHM (in radian) and θ is diffraction angle (in radians).

The amount of defect in the sample can be estimated from:

$$\delta = \frac{1}{D^2} \quad (6)$$

where D is average particle size and δ is dislocation density.

RESULTS AND DISCUSSION

Crystal structure and size determination

The X-ray diffraction patterns of the synthesized $CaAl_2O_4{:}Mn^{2+}$ nanocrystals is shown in Figures 2a and b. Six prominent peaks were observed in the diffractograms around 2θ values of 33.63, 30.08, and 18.22° corresponding to (124), (201), (110) for CAU and 30.15, 25.53 and 18.29° corresponding to (220), (111), (110) for CAP (Table 1). All the planes can be indexed to $CaAl_2O_4$. Structural identification of the nanomaterials from the XRD revealed monoclinic structure of the Mn^{2+} doped calcium aluminate nanophosphor. The high intensity of the peaks reveals the high crystallinity of the synthesized nanomaterials (Arunachalam, 2012). Average crystal size calculated from three prominent peaks show that the unpassivated sample, CAU, has the largest crystal size of 41.49 nm as a result of low strain and dislocation in the crystals; while the passivated sample, CAP, has 34.81 nm due to high dislocation and strain in the crystals. This is an indication that the presence of urea assists in the dissolution and combustion of the particles leading to increased crystal defect and strain. Urea has been applied in the preparation of nanomaterials using solution combustion synthesis (Qui et al., 2007; Krsmenovic et al., 2007). All these led to a homogeneous system with blended morphology and enhanced luminescence with reduced particle size. This of course is evident in the present paper.

Surface morphology study

The SEM micrograph unveils the foamy nature of the passivized CAP with wide particle distributions. The unpassivized CAU reveals the cluster spherical nature of the crystals interconnected by nanorods which could be due to poor dissolution of the particles (Figure 3a and b).

Photoluminescence studies

The ability of the nanoparticles to absorb incident energy and convert it into visible radiation was confirmed by PL investigation. Photoluminescence emission spectrum at 345 nm excitation shows three distinct peaks centered at 406, 454 and 493 nm for CAP with the maximum intensity obtained at 454 nm (Figure 4). Four distinct peaks were

Table 1. The structural data of sample CAP and CAU.

Sample ID	2θ(°)	FWHM (°)	Interplanar Spacing 'd ' (A°)	Plane (hkl)	Intensity	Average crystal size (nm)	Average dislocation density (lines/m)	Average crystal strain
CAP	30.15	0.3296	2.964	220	644.0	34.81	9.87×10^{-4}	2.82×10^{-1}
	25.53	0.1978	3.500	111	542.2			
	18.29	0.1978	4.869	110	604.6			
CAU	33.57	0.1978	2.673	124	574.5	41.49	8.73×10^{-4}	2.3×10^{-1}
	30.08	0.3296	2.969	201	617.1			
	18.22	0.1319	4.884	110	583.7			

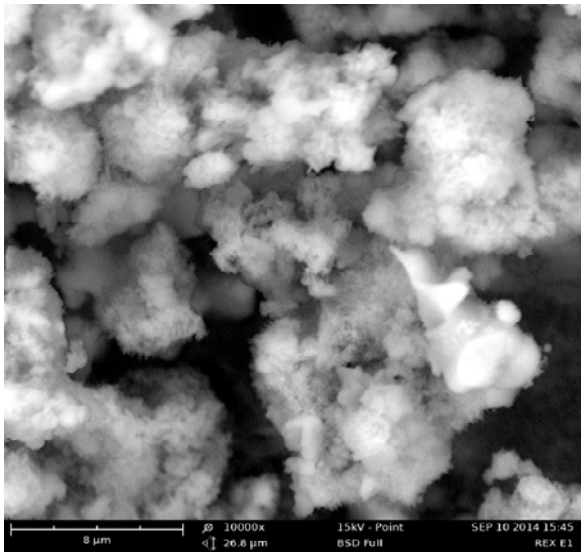

(a)

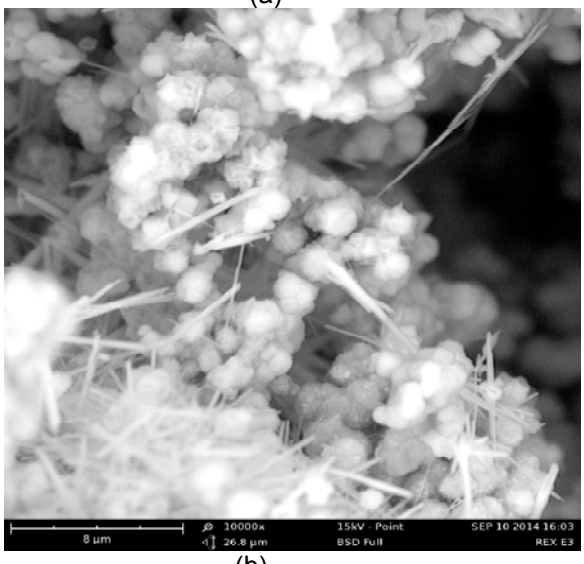

(b)

Figure 3. The SEM micrograph analysis of sample (a) CAP (b) CAU nanocrystals.

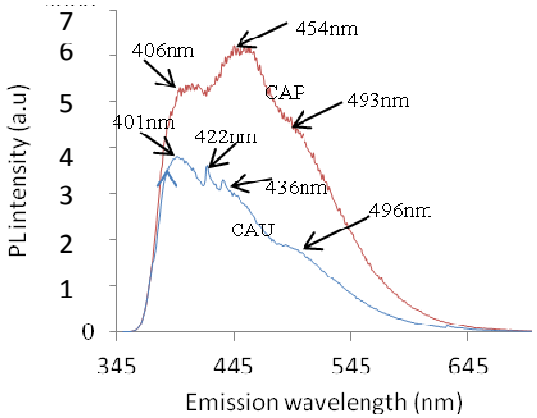

Figure 4. Photoluminescence emission spectra of the samples at 345 nm excitation.

obtained at 401, 422, 436 and 496nm respectively for CAU with the maximum intensity coming from 401 nm. All the peaks are in good agreement with the well-known Mn^{2+} emission transitions (Jubu et al., 2015). The emission wavelengths indicate characteristic blue emission which is typical of Mn^{2+}. Similar blue emission wavelengths were also obtained by Lin et al. (2008). The luminescent intensity of the thermal treated products varied appreciably with the presence of urea as CAP has the highest luminescence intensity. The emission intensity of the nanomaterials vary with crystal size such that CAU with high crystal size has a low emission intensity. According to (Dhlamini, 2008) the emission colors of phosphors vary with crystallite size. This is evident on CAU with dominant violet (380-450) nm emission peaks, and a low blue (450-495) nm emission peak due to high particle size of 41.49 nm; and CAP with deep blue emission peaks as a result of reduced particle size of 34.81 nm (Jagjeet et al., 2002) obtained blue-green emission on the phosphor at 254 nm UV excitation. The blue emission originates from the electron-hole recombination of self-trapped exciton (Yit-Tsong, 2002).

As can be seen on Figure 5, the samples showed unique responds to different excitation wavelengths. The CAP sample has low responses at 320 and 395 nm. The presence of urea seemingly enhanced the sensitizers of the CAP sample giving them better responses to a wide range of excitation wavelengths as a result of reduced

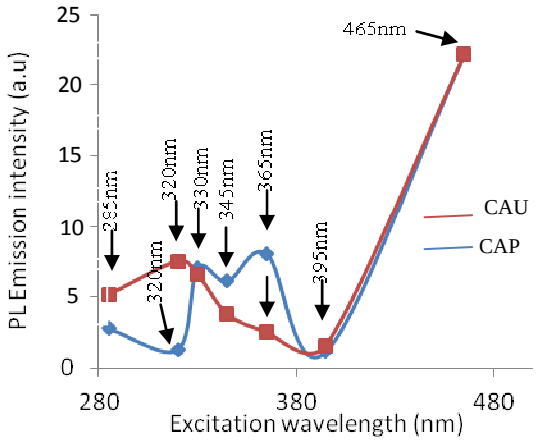

Figure 5. Plot of excitation wavelengths against highest emission intensities.

particle size. The emission intensities of CAP fluctuates between 285 and 395 nm UV excitation doses but increased sharply at 465 nm excitation giving rise to the highest emission intensity.

The CAU sample, without urea, and with high crystal size responded poorly between 330 and 395 nm excitation. This is probably due to the high crystallite size and hence increased band gap leading to decrease photoluminescence intensity as a result of separation of exciton wave functions with the activator (Diane, 2002). The hindered overlap reduces the energy transfer rate from the exciton to the impurities and as a result the non-radiative decay rate is increased and therefore the photoluminescence efficiency is decreased. A sharp responds by sensitizers is also recorded at 465 nm excitation on CAU. The samples respond differently to different excitation wavelengths as a result of variation in their particle sizes. Equivalent responses are recorded at 330, 395 and 465 nm respectively. The significant effect of particle size on photoluminescence emission intensity of the samples is quenched at the highest excitation wavelength, 465 nm, which gave the sensitizers of both samples a similar highest responds.

Conclusion

The manipulation of morphology and particle size by urea, and the effect of crystal size on the photoluminescence of manganese doped calcium aluminate nanocrystalline material was successfully carried out. Study revealed that the presence of urea reduced the average crystallite size of CAU from 41.49 to 34.81 nm for CAP, with the prepared $CaAl_2O_4:Mn^{2+}$ samples being monoclinic in structure. The SEM micrograph of CAU revealed spherical particles connected by nanorods, while the SEM image of CAP unveiled the foamy nature of the nanocrystals. The emission color and intensity of the nanocrystals were observed to be crystal-size dependent with high luminescence intensity and deep blue emission peaks recorded on CAP; while low luminescence intensity, prominent violet peaks and a weak blue emission peak were registered on CAU. Particle size was observed to have no effect on photoluminescence emission intensity at 465 nm excitation wavelength.

Conflict of Interest

The authors have not declared any conflict of interest.

REFERENCES

Ali HW (2011). Preparation and Properties of Long Afterglow $CaAl_2O_4$ Phosphors Activated by Rare Earth Metal Ions. M.Sc Thesis, University of the Free State, Republic of South Africa, pp. 10–121.

Amita V, Srivastava AK (2011). Sol-gel Derived Nanostructural Zinc Oxide for Bright Luminescence in Ultraviolet and Visible Spectral Region. Indian J. Chem. 50:1697–1702.

Arunachalam L (2012). The Role of Sintering in the Synthesis of Luminescence Phosphor." Sintering of Ceramics, In Tech Publishers, Thandulam, Chennai, India, pp. 321-337.

Bo L, Chaoshu S, Zeming Q (2005). Potential White-Light Long-Lasting Phosphors: Dy^{3+} -Doped Aluminte. Appl. Phys. Let. 86:191111-191113.

Christine KS, Samson AN (2010). Effect of Fuels on the Combustion Synthesis of $NiAl_2O_4$ Spinel Particles. Iranian J. Mater. Sci. Eng. 7(2):36 -38.

Dejene FB, Bem DB, Swart HC (2010). Synthesis and Characterization of $CaAl_xO_y$: Eu^{2+} Phosphor Prepared Using Solution-Combustion Meth. J. Rare Earth 28:272-276.

Dhlamini MS (2008). Luminescence Properties of Synthesized PbS Nanoparticles." PhD Thesis, University of the Free State, South Africa.

Diane KW (2002). Particle Size Dependence on the Luminescence Spectra of Eu^{3+}:Y_2O_3 and Eu^{3+}:CaO. PhD Dissertation, Virginia Polytecnique Institute and State University, Blackburg, Virginia, pp. 1-154.

Haranath D, Pooja S, Harish C, Anwar A, Nitesh B, Halder SK (2010). Role of Boric Acide in Synthesis and Tailoring the Properties of Calcium Aluminate Phosphors. Mater. Chem. Phys. 101:163 -164.

Jagjeet k, Nemana S, Beena J, Vikas D, Ravi S, Huma NB (2002). TL Glow Curve Study, Kinetics, PL and XRD Analysis of Mn^{2+} Doped $CaAl_2O_4$ Phosphors. J. of Min. and Mat. Character Engin. 11:1081-1084.

Jubu PR, Onoja AD, Echi IM (2015). Doping Concentration Dependence of the Luminescence of Mn^{2+} Activated Calcium Aluminate Nanoparticles. Res. J. Phys. Sci. 3(3):1-4.

Kartik NS, Dhoble SJ, Swart HC, Kyeongsoon P (2012). Phosphate Phosphors for Solid-State Lighting. Springer Verlag Berlin Heidelberg, pp. 1-75

Kelvil WG (2013). Green Technology for Nanoparticles in Biomedical Applications. CAB International, 1-108

Kenanakis G, Androulidaki KE, Savvakis C, Katsarakis N (2007). Photoluminescence of ZnO Nanostructures Grown by Aqueous Chemical Growth Technique. Superl. Microst. 42:473–478.

Krsmenovic R, Morozov V, Lebedev O, Polizzi S, Speghini A, Bettinelli M (2007). Structural and Luminescence Investigation on Gadolinium Gallium Garret Nanocrystalline Powders Prepared by Solution Combustion Synthesis. Nanotechnology 18:325604-325613.

Lin L, Min Y, Chao SS, Weiping Z (2008). Luminescence properties of a new red long-lasting phosphor: $MgSiO_4$:Dy^{3+}, Mn^{2+}. J. Alloys Comp, 455:327-330.

Madhukumar K, Rajendra KB, Ajith PKC, James J, Elias TS,

Padmanabhan V, Nair CMK (2006). Thermoluminescence Dosimetry of Rare Earth Doped Calcium Aluminate Phosphors. Bull. Mat. Sci. 29(2):119 -122.

Mou P, Umapada P, Justo MG, Jimenez Y, Felipe PR (2012). Effects of Crystallization and Dopant Concentration on the Emission Behavior of TiO_2:Eu Nanophosphors. Nanosc. Res. Let. **7**(1):1-12.

Nguyen NT, Nguyen MS, Phun TD (2004). Photoluminescence Characteristics of the $CaAl_2O_4$:Eu^{2+} Co-doped with Dy^{3+} Synthesized by Combustion Method." Int. J. Chem. Mat. Res. 2(8):7575–80.

Qui Z, Zhou Y, Lu M, Zhang A, Ma Q (2007). Combustion Synthesis of Long-Persistent Luminescent MaI_2O_4:Eu^{2+}, R^{3+} (M = Sr, Ba, Ca, R = Dy, Nd and La). Nanop. Lumines. Mech. Res. 55:2620-2626.

Rivas JM, De'Aza AH, Pena P (2004). Synthesis of $CaAl_2O_4$ from Powders –Particle Size Effect." J. Eur. Cera. Soc. 25:3269-3279.

Saeid K, Jalal R, Ehsan M, Mahmoud A, Arash D (2012). Syntheis and Characterization of Cr-Doped Al_2O_3 Nanoparticles Prepared Via Aqueous Combustion Method. Casp. J. Appl. Sci. Res. 1(13):16-22.

Satapathy kk, Mishra GC (2014). Hydrazine Assisted Self-combustion Synthesis of $CaAl_2O_4$:Eu^{2+} Phosphor and its Mechanoluminescence Characterization." Int. J. Sci, Basic Appl. Res, 16:188-196.

Senapati US, Jha DK, Sarkar D (2013). Green Synthesis and Characterization of ZnS Nanoparticles. Res. J. Phys. Sci. 1(7):1-6.

Sugaderan S (2013). Synthesis, Structural, and Dielectric Properties of Zinc Sulfide Nanoparticles. Int. J. Phys. Sci. 8(21):11-21.

Toniolo J, Lima M, Takimi A, Bergmann C (2005). Synthesis of Alumina Powders by the Glycine-Nitrate Combustion Process. Mater. Res. Bull. 40(3):561-569.

Toumas A, Jorma, Hogne, Mika L, Janne N (2012). Comparison of Sol-Gel and Solid State Prepared Eu^{2+} Doped Calcium Aluminates." Mat. Sci. 20(1):16-19.

Vijay S, Natarajan V, Jun-Jie Z (2007). Luminescence and EPR Investigations of Mn Activated Calcium Aluminate Prepared via Combustion Method. Sci. Direct Opt. Mat. 30:468 -472.

Yit-Tsong C (2002). Size Effect on the Photoluminescence Shift in Wide Band-Gap Materials: A Case Study of SiO_2-Nanoparticles. Tamkang J. Sci Eng. 5(2):99 -106.

academicJournals

Vol. 10(19), pp. 543-548, 16 October, 2015
DOI: 10.5897/IJPS2015.4393
Article Number: 81162E455712
ISSN 1992 - 1950

http://www.academicjournals.org/IJPS

International Journal of Physical Sciences

Full Length Research Paper

Hydrothermal synthesis and structural characterization of an organically-templated open-framework trimolybdates

Chinyere A. Anyama, Grace E. Iniama, Joseph O. Ogar and Ayi A. Ayi*

Inorganic Materials Chemistry Laboratory, Department of Pure and Applied Chemistry, University of Calabar, P. M. B. 1115, Calabar, Nigeria.

Received 27 July, 2015; Accepted 2 October, 2015

A new one-dimensional coordination polymer formulated as $[C_2H_{10}N_2]$ $[Mo_3O_{10}]$, 1, has been synthesized under hydrothermal conditions in the presence of ethylenediamine. The surface morphology of the as-synthesized product reveals colorless rod-like single crystals of 1. The compound crystallizes in monoclinic space group $P2_1/n$ with a = 8.08 Å, b =14.39 Å, c = 8.89 Å; β = 97.76°, V = 1033.65(12) Å3, Z = 4. The structure is a one-dimensional chain consisting of $[Mo_3O_{10}]^{2-}$ clusters of Mo (VI) octahedral interspersed by the amine molecules. In the infrared spectrum of the compound, the symmetric stretching vibrational mode of the -NH_2 group is observed at 3278 cm^{-1}, while the band at 1604 cm^{-1} is assigned to scissoring mode of the –NH_2 group. The peaks in the spectral range 1913 -2492 and 2962 cm^{-1} are attributed to -CH_2 symmetric and asymmetric stretching vibrations respectively. The absorption bands at 1404 cm^{-1} is due to scissoring, while the one at 1149 cm^{-1} is attributable to twisting modes of - CH_2 group . The characteristic band of the stretching vibrational modes of the Mo=O double bonds is observed at 1018 cm^{-1}, while the vibrational stretching frequency involving single Mo-O bonds is observed at 846 cm^{-1} and the scissoring mode of this bond is at 542 cm^{-1}.

Key words: Hydrothermal synthesis, amine-templated molybdates, molybdenum oxide-organic frameworks, one-dimensional chain.

INTRODUCTION

The great interest in the design of molybdenum(VI) oxide−organic frameworks (MOOFs) is not only due to their applications in such areas as catalysis , magnetism, sorption etc ., but also due to its fascinating structural chemistry (Lysenko et al ., 2010; Pope and Müller , 2001; Senchyk et al., 2014). Various synthetic approaches have been used to isolate highly crystalline samples suitable for structural characterization by X-ray diffraction, but the synthesis of organic−inorganic hybrids using hydrothermal conditions has received special attention in the field of coordination solids based on transition-metal oxides, including transition-metal molybdate complexes (Asnani et al., 2012; Hagrman and Zubieta, 1998; Hagrman et al., 1999; Randy et al., 2001; Hagrman and Zubieta, 2000).

*Corresponding author. E-mail: ayiayi72@gmail.com, a.anyama@chem.unical.edu.ng.

Hydrothermal method is a synthesis pathway in which products are produced using thermal (heat) energy and aqueous solvent. The success of this method is derived from the extremely solvating ability owing to reduced viscosity of the water under these conditions. This allows the dissolution and mixing of the solid reagents thereby minimizing differential solubility problem (Davis, 1992; Barrer, 1982; Francis and O'Hare, 1998). It has been demonstrated that the hydrothermal chemistry of polyoxomolybdates involves many interrelated reaction variables, including the pH, the molybdenum source, and the identities of other reaction species, the temperature, and time (Wu et al., 2002; Xu et al., 2000; Zhang et al., 2007; Zhang et al., 2015; Hubbard et al., 2008). Molybdophosphonates as building blocks or subunits in extended structures have been studied (Hubbard et al., 2008; Armatas et al., 2008; Jones et al., 2010; Armatas et al., 2009). A molybdenum diphosphonate network structure exhibiting reversible dehydration and selective uptake of methanol have also been reported and it is the first molybdenum diphosphonates in the absence of co-ligands (Ayi et al., 2013).

MATERIALS AND METHODS

The syntheses were carried out in Ace pressure tubes (15 cm^3), purchased from Aldrich Chemical Co., and heated in programmable ovens. The reagents used for syntheses were obtained from Aldrich (Hexaamomoium heptamolybdate tetrahydrate $(NH_4)_6Mo_7O_{24}\cdot 4H_2O$; ethylenediamine,) or Epsilon Chime (4-carboxyphenylphosphonic acid) and used without further purification. In a typical synthesis of **1**, $(NH_4)_6Mo_7O_{24}\cdot 4H_2O$ (0.3088 g, 0.25 mmol) was stirred together with 4-carboxyphenyl phosphonic acid (0.101 g, 0.5 mmol) in 5 cm^3 of distilled water. This was followed by the addition of 0.02 cm^3 of ethylenediamine and the pH of the solution was adjusted to 3 by dropwise addition of 0.2 cm^3 of Conc HCl. The resultant mixture was homogenized for 30 min before transferring into the reaction vessel and heated in an oven at 120°C for 8 h. The product, a crop of colorless crystalline material was washed with distilled water and air-dried.

Characterization

The surface morphology of the as-synthesized compound was determined using computer controlled polarized PZPZ300T-8M electron microscope. The ultraviolet-visible measurements were recorded with the help of Thermo Scientific Evolution 201 UV-vis spectrophotometer. The Infrared spectra were recorded on a Shimadzu IR affinity-1 from 400 to 4000 cm^{-1}.

Crystal structure

"X-ray diffraction data was collected on an Oxford Diffraction Gemini diffractometer fitted with an Atlas CCD detector using Mo-Kα radiation of wavelength 0.71073 Å at 150 K". The crystal structure and refinement parameters are given in Table 1. "The structure was solved using SHELXS-97 and refined using full-matrix least squares in SHELXL-97 (Sheldrick, 2008). The final refinements were generally straight forward with all non-hydrogen atoms refined anisotropically in the final least squares run, and hydrogen atoms included at calculated positions".

RESULTS AND DISCUSSION

We were interested in isolating Mo (VI) oxide cluster as a building block in the preparation of molybdo-carboxyphosphonate frameworks. During the investigation of the $(NH_4)_6Mo_7O_{22}\cdot 4H_2O$ –HCl Carboxyphenylphosphonic acid–ethylenediamine–H_2O–system, a new inorganic-organic hybrid material, $(C_2H_{10}N_2)$ (Mo_3O_{10}) constructed from molybdenum (VI) oxide with encapsulated ethylenediammonium ions was isolated. The carboxyphenylphosphonic acid was added into the reactant mixture with the aim of obtaining molybdenum organophosphonate frameworks, but was not incorporated into the final product. The ethylenediamine added to the synthetic gel exerts a significant structural role in controlling the architecture of the molybdenum oxide phase formed as well as compensating the metal oxide anionic charge. The addition of the HCl helps in maintaining acidic pH before and after the reaction. It is only in an acidic medium that the amine component gets protonated. A portion of the soluble reactant precursor was taken out for UV-Vis measurement. The UV-Vis spectrum of the reactants in aqueous solution is presented in Figure 1. The spectrum exhibits three absorption bands at 279, 284 and 286 nm. The strong band at 279 and 284 nm are attributable to π- π* transitions. These transitions involves moving electron from a bonding pi-orbital to an antibonding pi-orbital and is said to occur at high energy region of 35,842 to 35211 cm^{-1}. The broad band at 286 nm corresponds to n – π* transitions, which involve moving an electron from a non-bonding electron pair to an antibonding pi-orbital and is found to occur at lower energy region of 34,364 to 34,965 cm^{-1}

The surface structure and morphology of the as-synthesized product reveals colorless rod-like crystals (Figure 2). The crystal data and structure refinement parameter for compound **1 is** presented in Table 1. The compound crystallizes in monoclinic space group $P2_{1/n}$ (No. 14) with a = 8.08 Å, b =14.39 Å, c = 8.89 Å; β = 97.76°. The asymmetric unit (Figure 3) consists of Molybdenum center in octahedral coordination by six oxygen atoms, and protonated amine. The bridging Mo-O bond lengths in the range of 1.592(16) to 1.693(15) Å are shorter compared with the terminal Mo-O bonds (1.994(5) to 2.429(14) Å) and the O(1)-Mo(1)-O(#2) bond angles in the range of 158.10 to 170.3997° are in good agreement with similar reported compounds (Hubbard et al., 2008; Ayi et al., 2013). The structure is a one-dimensional chain consisting of $(Mo_3O_{10})^{2-}$ clusters interspersed by the ethylenediammonium cation (Figure 4), which also serves to compensate the framework negative charge of -2.

Figure 5 gives the infrared spectrum of compound **1**. In this spectrum, the two peaks at 3657 and 3780 cm^{1}

Table 1. Crystal data and structure refinement for **1**.

Empirical formula	$C_2H_{10}N_2Mo_3O_{10}$
Formula weight	254.91
Temperature / K	150(2)
Wavelength / Å	0.7107
Crystal system	Monoclinic
Space group	*P2(1)/n (No.14)*
Unit cell dimensions	*a* = 8. 08(8)Å, alpha = 90°
	b = 14.39(3)Å, beta = 97.76(4)°
	c = 8.89(4)Å, gamma = 90°
Volume / Å^3	1033.65(12)
Z	4
Density (calculated) / g cm^{-3}	1.972
Absorption coefficient / mm^{-1}	1.595
F(000)	1502
Crystal size / mm	0.18 × 0.05 × 0.02
Theta range for data collection	2.97 to 29.96°
Index ranges	–22 ≤ *h* ≤ 27; –14 ≤ *k* ≤ 13; –11 ≤ *l* ≤ 12
Reflections collected	6916
Independent reflections	2442 (*R*(int) = 0.0284)
Reflections observed (>2)	1502
Data Completeness	0.905
Absorption correction	Semi-empirical from equivalents
Max. and min. transmission	1.00000 and 0.94878
Refinement method	Full-matrix least-squares on F^2
Data / restraints / parameters	1902 / 0 / 156
Goodness-of-fit on F^2	0.902
Final R indices (*I* > 2 (*I*))	R_1 = 0.0390 wR_2 = 0.0405
R indices (all data)	R_1 = 0.0571 wR_2 = 0.0587
Largest diff. peak and hole / e Å^{-3}	0.988 and -1.057

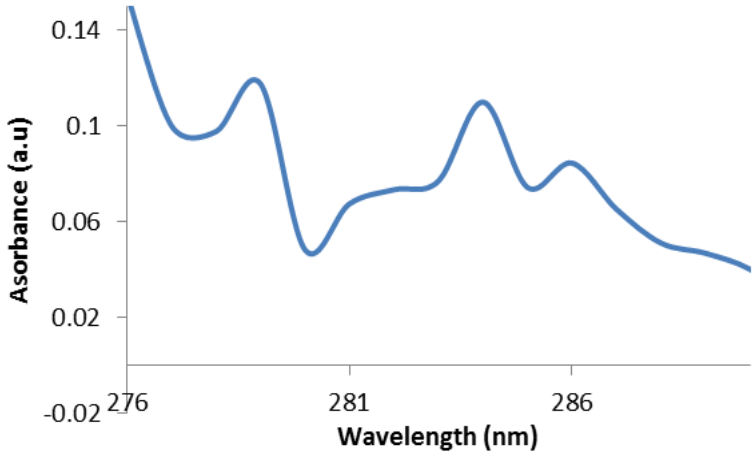

Figure 1. UV-Vis spectrum of the reactant mixture in aqueous solution for the synthesis of **1**.

superimposed on the water peak can be attributed to -NH_2asymmetricstretching involved in N-H…O hydrogen bond formation . The symmetric stretching vibrational mode of the -NH_2 group is observed at 3278 cm^{-1}, while

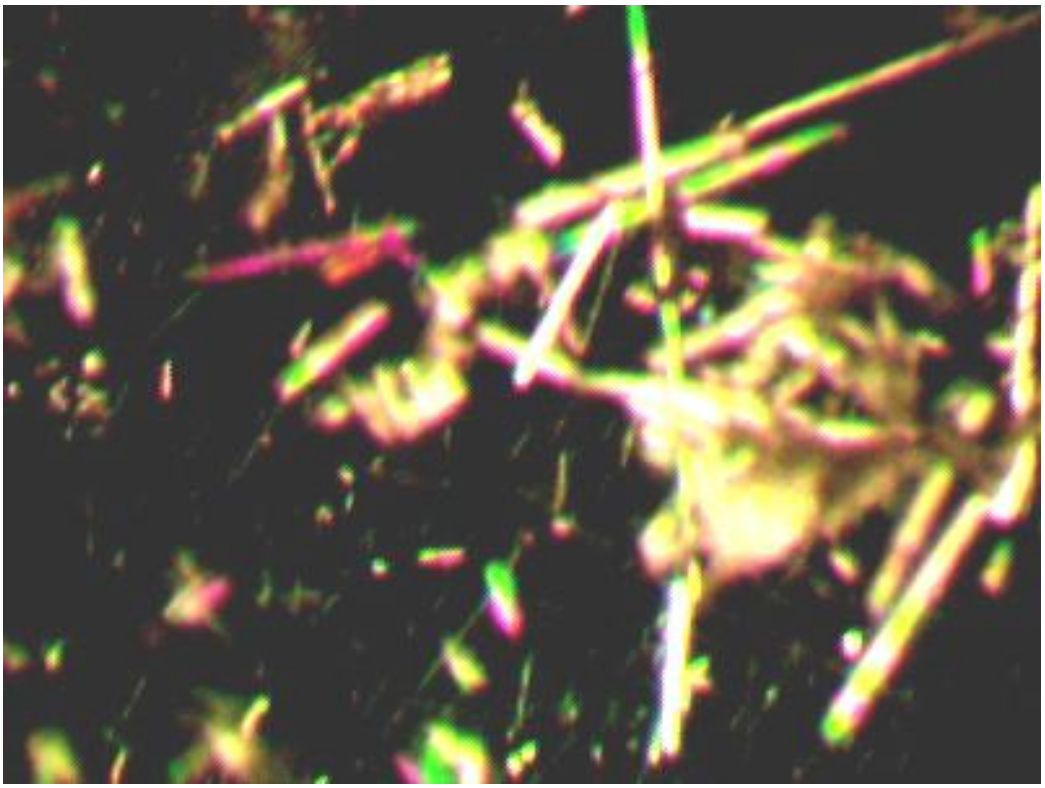

Figure 2. Optical microscopic image of the as-synthesized compound **1**.

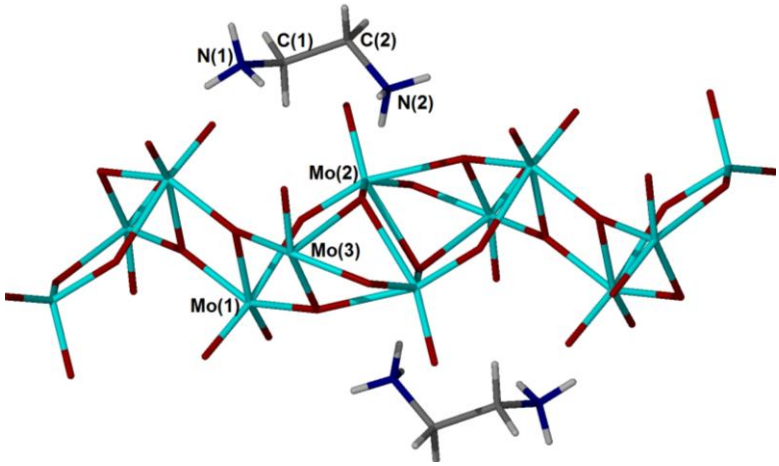

Figure 3. The structure of **1** showing the coordination environment of Mo and the encapsulated amine molecule.

the band at 1604 cm $^{-1}$ is assigned to scissoring mode of the $–NH_2$ group. The peaks in the spectral range 1913 - 2492 and 2962 cm $^{-1}$ are attributed to $-CH_2$ symmetric and asymmetric stretching vibrations respectively. The absorption bands at 1404 cm $^{-1}$ is due to scissoring, while the one at 1149 cm^{-1} is attributable to twisting modes of - CH_2 group . The characteristic band of the stretching vibrational modes of the Mo=O double bonds is observed at 1018 cm^{-1} and compares well with similar compounds in the literature (Hubbard et al., 2008). The vibrational stretching frequency involving single Mo-O bonds is observed at 846 cm^{-1} while the scissoring mode of this bond is at 542 cm^{-1}. The various assignments are made on the basis of similar work in the literature (Asnani

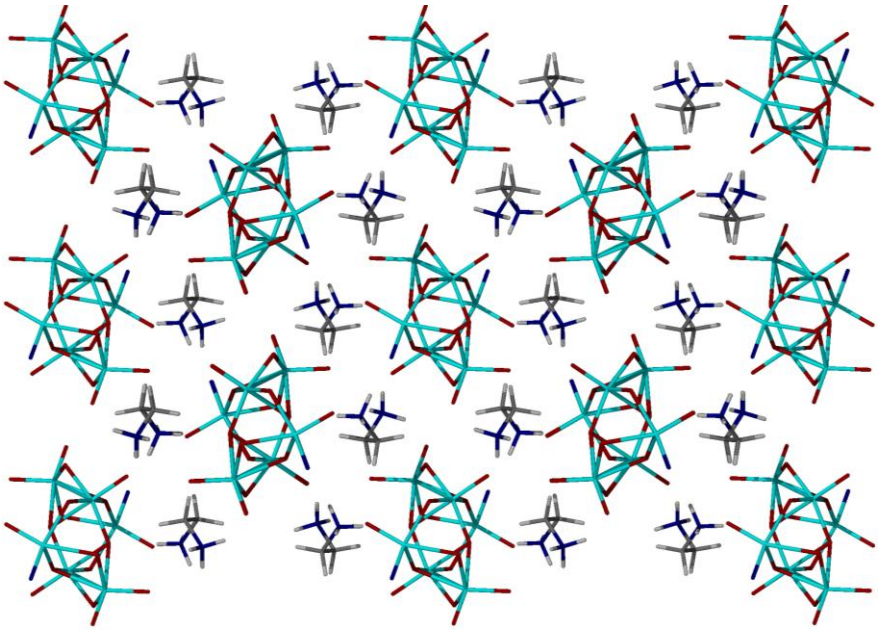

Figure 4. Structure of **1** viewed along the (100) direction showing the $(Mo_3O_{10})^{2-}$ clusters interspersed by the ethylenediammonium cation.

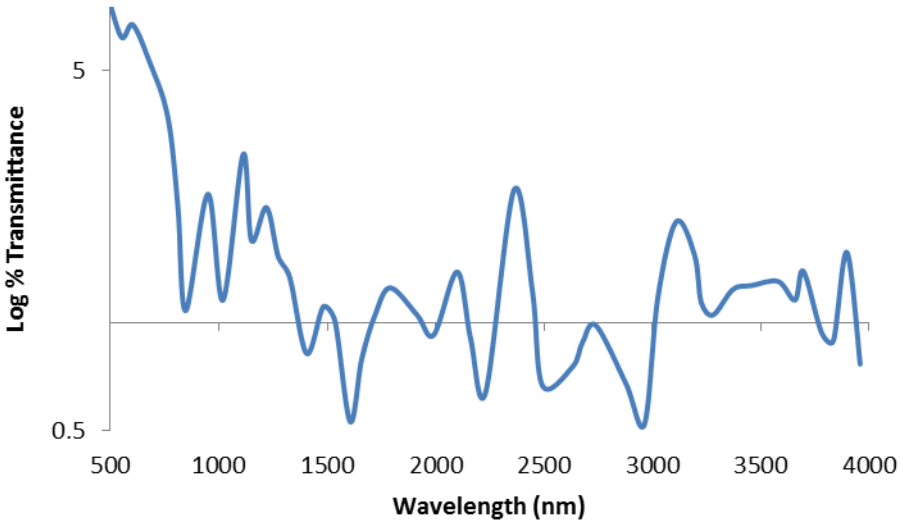

Figure 5. The infrared spectrum of $(C_2H_{10}N_2)$ (Mo_3O_{10}), **1** .

et al., 2012; Hagrman and Zubieta, 1998; Hubbard et al., 2008; Sierka et al., 2007).

Conclusion

In conclusion, a new one-dimensional coordination polymer formulated as $(C_2H_{10}N_2)$ (Mo_3O_{10}), has been synthesized under hydrothermal conditions in the presence of ethylenediamine. The surface structure and morphology of the as-synthesized product reveals colorless rod-like crystals. The structure is a one-dimensional chain consisting of $(Mo_3O_{10})^{2-}$ clusters of Mo (VI) octahedral interspersed by the amine molecules. In the IR spectrum, the two peaks at 3657 and 3780 cm^{-1} superimposed on the water peak can be attributed to $-NH_2$ asymmetric stretching involved in N-H…O hydrogen bond formation . The protonated organic amine interacts with the inorganic frameworks through multiple hydrogen bonds of the type N-H…O. Efforts are

under way to use this compound as a building block in designing Mo (VI) oxide-carboxyphosphonate framework materials.

Conflict of Interest

The authors declare that there is no conflict of interest in publishing this article.

ACKNOWLEDGEMENT

This work was supported by The World Academy of Sciences for the Advancement of Science in developing countries (TWAS) under Research Grant No 12-169 RG/CHE/AF/AC-G -UNESCO FR: 3240271320 for which grateful acknowledgment is made. A.A.A is also grateful to the Royal Society of Chemistry for personal Research grant. The authors are thankful for the support of Andrew Burrows of University of Bath, UK, for the Single-Crystal X-ray crystallographic data.

REFERENCES

Armatas NG, Allis DG, Prosvirin A, Carnutu G, O'Connor CJ, Dunbar K, Zubieta J (2008). Molybdophosphonate clusters as building blocks in the oxomolybdate-organodiphosphonate/Cobalt(II)-organoimine system. Structural influences of secondary metal coordination preferences and diphosphonate tether lengths. Inorg. Chem. 47:832.

Armatas NG, Ouellette W, Whitenack K, Pelcher J, Liu H, Romaine E, O'Connor CJ, Zubieta J (2009). Construction of Metal-Organic Oxides from molybdophosphonates clusters and copper bipyrimidine building blocks. Inorg. Chem. 48:8897-8910.

Asnani M, Kumar K, Duraisamy T, Ramanan A (2012). Crystallization of organically templated phosphomolybdate cluster-based solids from aqueous solution. J. Chem. Sci. 124:1275-1286.

Ayi AA, Burrows AD, Mahon MF, Sebastian VM (2013). A molybdenum diphosphonate network structure exhibiting reversible dehydration and selective uptake of methanol. Cryst. Eng. Comm. 15:9301-9303

Barrer RM (1982). Hydrothermal Chemistry of Zeolites, Academic press, London.

Davis, Lobo (1992). Zeolite and molecular sieve synthesis, J. Chem. Mat. 4:756-768.

Francis RJ, O'Hare D (1998). The kinetics and mechanisms of the crystallization of microporous materials. J. Chem. Soc. Dalton Trans. 1998:3133-3148

Hagrman D, Zubieta J (1998). Organic-inorganic composite oxide phase: one-dimensional molybdenum oxide chains entrained within a three-dimensional complex cationic framework in ({Cu_2(triazolate)$_2$(H_2O)$_2$}Mo_4O_{13}). Chem. Commun. 1998:2005-2006.

Hagrman PJ, Hagrman D, Zubieta J (1999). Organic-Inorganic hybrid Materials: From "Simple" Coordination Polymers to Organodiamine-Templated Molybdenum oxide. Angew. Chem. Int. Ed. 38:2638-2684.

Hagrman PJ, Zubieta J (2000). Solid-state coordination chemistry: Influences of {M(terpyridyl)} (M = Ni(III), Cu(II), Ni(II)} subunits on molybdenum oxide structures. Inorg. Chem.39: 5218−5224.

Hubbard DJ, Johnston AR, Casalongue HS, Sarjeant AN, Norquist AJ. (2008). Synthetic Approaches for Noncentrosymmetric Molybdates. Inorg. Chem. 47:8518-8525

Jones S, Liu H, Schmidtke K, O'Connor CC, Zubieta J, (2010). A bimetallic oxide ({$Cu(bpy)$}$_2Mo_4O_{10}$($O_3PCH_2C_6H_4CH_2PO_3$)$_2$), Constructed from novel ($Mo_4O_{10}(O_3PR)_4$}$_n^{4n-}$ chains. Inorg. Chem. Comm. 13:298.

Lysenko AB , Senchy G A , Lincke J , Lässig D , Fokin AA, Butova ED, Schreiner PR, Krautscheid H, Domasevitch KV (2010). Metal oxide-organic frameworks (MOOFs), a new series of coordination hybrids constructed from molybdenum (VI) oxide and bitopic 1,2,3-triazole linkers. Dalton Trans. 39:4223−4231.

Pope MT , Müller A (2001). Polyoxometalate Chemistry from Topology via Self-Assembly to Applications. Kluwer Academic: Dordrecht, Netherlands.

Randy S, Rarig J, Zubieta J (2001). Influences of secondary metal–ligand subunits on molybdenum oxide structures: the hydrothermal syntheses and structures of ($M(tpytrz)_2Mo_4O_{13}$) (M = Fe, Co, Ni, Zn; tpytrz = tripyridyltriazine), ($Ni(tpytrz)Mo_2O_7$) and ($Zn_2(tpytrz)Mo_2O_8$). Dalton Trans. 23:3446−3452.

Senchyk GA , Lysenko AB , Babaryk AA , Rusanov EB , Krautscheid H , Neves P , Valente AA , Gonçalves IS , Krämer KW , Liu SX, Decurtins S, Domasevitch KV (2014). Triazolyl−Based Copper−Molybdate Hybrids: From Composition Space Diagram to Magnetism and Catalytic Performance. Inorg. Chem. 53:10112−10121

Sheldrick GM (2008). A short history of SHELX. Acta Cryst. 64:112.

Sierka M, Todorova TK, and Sauer J, Kaya S, Stacchiola D, Weissenrieder J, Shaikhutdinov S, and Freund H-J, (2007) Oxygen adsorption on Mo„112… surface studied by ab initio genetic algorithm and experiment . J. Chem. Phys. 126:234710

Wu CD, Lu CZ, Zhuang HH, Huang JS (2002). Hydrothermal assembly of a novel three-dimensional framework formed by ($GdMo_{12}O_{24}$)$^{9-}$ anions and nine coordinated Gd^{III} cations. J. Am. Chem. Soc. 124:3836-3837.

Xu Y, Xu JQ, Zhang KL, Zhang Y, You XZ (2000). Keggin unit supported transition metal complexes: Hydrothermal synthesis and Characterization of (Ni(2,2'-bipy)3)1.5(PW12O40Ni(2,2'-bipy)$_2$(H_2O))$_{0.5}H_2O$ and (Co(1,10'-phen)$_3$)$_{1.5}$ ($PMo_{12}O_{40}$Co(1,10'-phen)$_2$(H_2O)))·0.5H_2O. Chem. Comm. 2:153-154.

Zhang JW, Kan XM, Li XL, Luan J, Wang XL (2015). Transition metal carboxylate coordination polymers with amide-bridged polypyridine co ligands: assemblies and properties. Cryst. Eng. Comm. 17:3881-3907

Zhang YY, Qi Y, Zhang Y, Liu ZY, Zhao YF, Liu ZM (2007). Synthesis, structure and magnetic properties of a new iron phosphonate-oxalate with 3D framework: ($Fe(O_3PCH_3)C_2O_4$)(0.5)(H_2O)). Mat. Res. Bull. 42:1531.

International Journal of Physical Sciences

Related Journals Published by Academic Journals

- *African Journal of Pure and Applied Chemistry*
- *Journal of Internet and Information Systems*
- *Journal of Geology and Mining Research*
- *Journal of Oceanography and Marine Science*
- *Journal of Environmental Chemistry and Ecotoxicology*
- *Journal of Petroleum Technology and Alternative Fuels*

academicJournals